

Reports

Geologic Evidence for Recurrent Moderate to Large Earthquakes Near Charleston, South Carolina

Abstract. Multiple generations of earthquake-induced sand blows in Quaternary sediments and soils near Charleston, South Carolina, are evidence of recurrent moderate to large earthquakes in that area. The large 1886 earthquake, the only historic earthquake known to have produced sand blows at Charleston, probably caused the youngest observed blows. Older (late Quaternary) sand blows in the Charleston area indicate at least two prehistoric earthquakes with shaking severities comparable to the 1886 event.

The seismic record of the southeastern United States is dominated by the 1886 Charleston, South Carolina, earthquake (modified Mercalli intensity IX to X, estimated body-wave magnitude $m_b = 6.6$ to 7.1) (1, 2), which was the strongest historic earthquake in that area. The determination of the time and location of any future earthquakes as large as the 1886 event is a major consideration in the engineering design of facilities in the Southeast. However, the causative mechanism of the 1886 earthquake (and

southeastern seismicity in general) remains uncertain although seismotectonic hypotheses abound (3).

Because of this uncertainty and because the 300-year historic seismic record is shorter by an order of magnitude than present estimates of the recurrence interval of major earthquakes in the region (4), we have sought to extend the seismic record in the Charleston area by a field search for earthquake-induced, liquefaction-flowage features called "sand blows" (5). Sand blows result

from the liquefaction and subsequent venting to the ground surface of subsurface water-saturated sediment. They occur as small sand mounds (sand volcanoes) and as sand-filled fissures or craters surrounded by surficial sheets of ejected sand. We have recognized sand blows near Charleston that probably were caused by the 1886 earthquake and sand blows that represent two or more prehistoric earthquakes (6).

The 1886 earthquake produced abundant sand-blow craters throughout its meizoseismal zone (Fig. 1) (1) and scattered liquefaction-related features up to 100 km from Charleston (7). Near Charleston, fluidized sand beds vented explosively into the air and produced large craters and surrounding blankets of ejected sand. Figure 2a is a photograph of a typical 1886 crater and sand blanket about 0.3 m thick around the crater's rim. Crater filling had begun by the time the photograph was taken; clasts of dark soil are scattered in the bowl-shaped crater, and some of the sand blanket is sloughing into the crater. Cox and Talwani (8) recently excavated an 1886 sand blow that consists of a thin ejection blanket and a sand-filled fissure through which the sand was ejected; weathering of the sands in the ejection blanket has been minimal.

We have found numerous sand blows in a drainage ditch system near Hollywood (Fig. 1), within the region reported to contain many 1886 sand blows (1). The 2- to 3-m-deep ditch is cut into upper Pleistocene barrier and nearshore marine sands and their superimposed soil profiles. These soils are spodosols characterized downward below thin surficial O and A horizons by a light gray E horizon, a thick (0.5 to 1.5 m) Bh horizon, and a B-C horizon. Below the solum, C horizon sands grade downward into less weathered Pleistocene sediments. The solum and C horizons contain, and locally are developed in, the sand-blow sediments.

Figure 2, b and c, shows a representative filled sand-blow crater, one of dozens of similar features exposed in the ditch. Soil horizons are cut by an irregularly bowl-shaped crater containing bedded and nonbedded layers of fine to medium sand and clasts of Bh material. The Bh and B-C horizons are much thinner within the filled crater than to either side. Beneath its Bh and B-C horizons, the filled crater contains a structureless, very light gray sand with only slight humate staining (layer 5), which overlies a sequence of thinly bedded, light- and dark-colored sands (layer 4). The lowermost stratum of the bedded

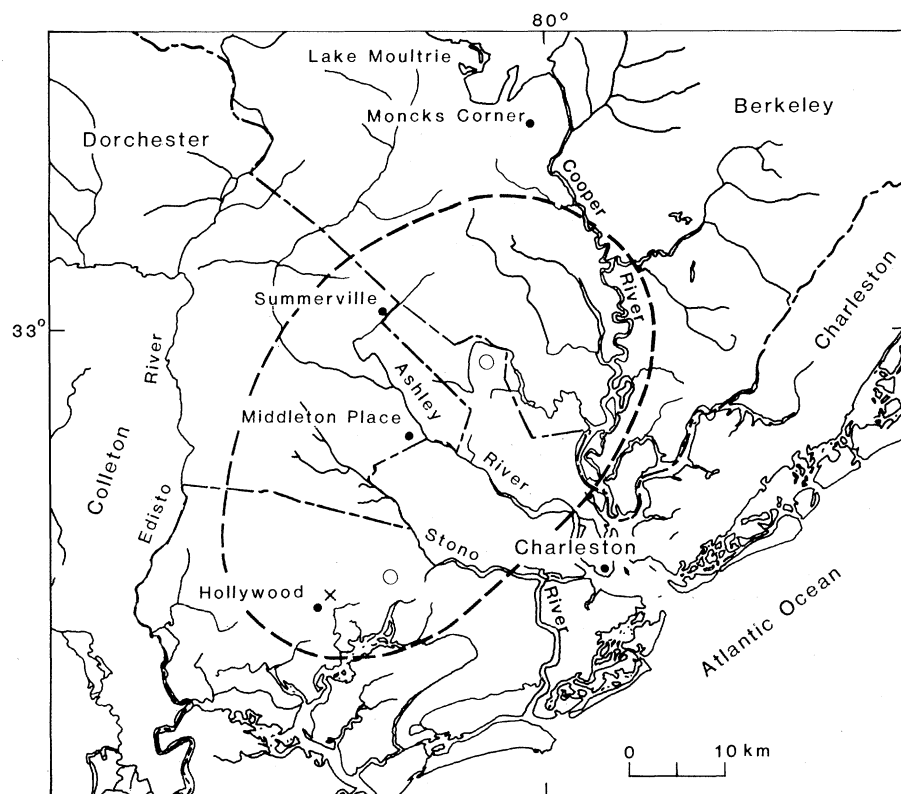


Fig. 1. Map of the area near Charleston, South Carolina, showing the counties, the meizoseismal zone of the 1886 earthquake (the area within the dashed lines), and the study site; ○, centers of highest intensity of the 1886 earthquake (1); x, site where multiple liquefaction-induced flowage features were examined.

sequence sharply overlies a medium light gray sand containing many small clasts of Bh material, wood, plant material, and some clasts(?) of light-colored sand (layer 3). This clast-rich layer grades down into a structureless zone (layer 2) that contains only scattered small Bh and light-colored sand clasts. Layer 2 grades down into another sand (layer 1) containing densely packed small and large clasts (up to 20 cm) of Bh material. At and below the thinly bedded sequence, the sides of the crater are sharply defined by a color boundary and by the presence of clasts within the crater. Lateral excavations into the bank here and elsewhere showed that the filled craters are roughly circular to elliptical in plan view.

The feature shown in Fig. 2, b and c, is interpreted as a filled sand-blow crater similar in size and origin to the 1886 crater-type sand blows (Fig. 2a). Recogn-

izable phases in the development of these craters include the following: (i) excavation of an initial large hole by an explosive discharge of sand, humate-rich soil, and water; (ii) continued expulsion of fluidized sand after the explosion; (iii) churning of sand, soil clasts, and water in the bowl and throat of the exploded hole followed by the settling of larger particles as the upward flow of water diminished; and (iv) slow filling of the upper part of the crater during the weeks or months after the flowage stopped.

The initial explosive phase is represented by the bowl-shaped unconformity between the sediment now in the crater and preexisting soil units (Fig. 2c). An ejection blanket probably formed around the crater during and after the explosion, but subsequent development of the soil profile has obscured its sedimentary record.

The three layers of sand and soil clasts below the bedded sequence consist of sediments trapped at the bottom of the crater during the loss of pore-water pressure. The clasts were segregated in the churning fluidized mixture when the largest (or densest) particles settled into layer 1 and the smaller (or lighter) particles were carried upward into layer 3. The bedded sequence and the structureless sand above it probably represent slow filling of the crater (as in Fig. 2a) after the liquefaction-flowage event as sediments washed in during rains and slumped from the crater's rim.

Although injection of fluidized sands into the craters obviously occurred, a geologic record of the intrusion is generally obscured. As the pore pressure dissipates and upward flow ceases at the end of an eruption, structures produced by the downward settling of soil clasts

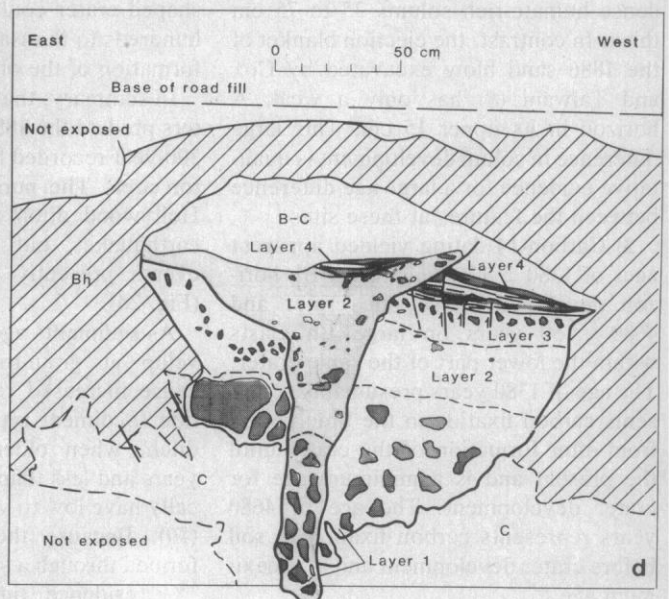
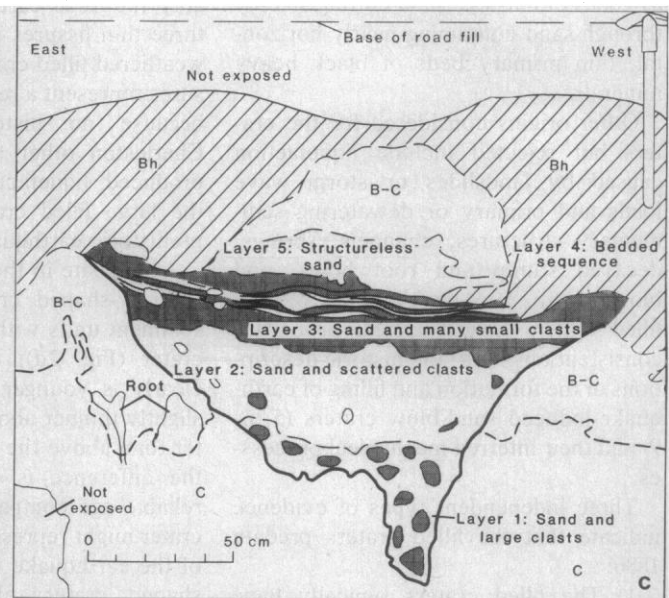


Fig. 2. (a) Typical sand-blow crater photographed near Charleston, South Carolina, in 1886. [Photograph from the Charleston Museum] (b) Typical filled sand-blow crater in a ditch near Hollywood, South Carolina (see Fig. 1). (c) Descriptive sketch of the filled crater in (b). Description of the Bh horizon: sand, quartzose, humate-cemented, fine to medium, brownish-black, massive; the B-C horizon: sand, quartzose, fine to medium, pale reddish-brown, friable, structureless (single grain); and the C horizon: sand, quartzose, fine to medium, yellowish-gray, friable, structureless (single grain). (d) Cross-cutting sand blows. The soil and layer descriptions are the same as in (c).

and sand replace structures formed during upward flow; weathering and mottling of the C horizon further obliterates evidence for injection. Several lines of evidence suggest that the source bed (liquefied zone) for the mobilized sand is the C horizon and underlying slightly weathered sands. In one filled crater, sand can be traced through the C horizon as stringers extending into and through the basal zone of large clasts within the crater. In another example, a large coherent block of solum (about 1 m² as seen on the ditch wall) foundered into the liquefied C horizon directly below a filled crater. Fewer clasts of soil-horizon material are within this crater than are typically present, and C horizon sand can be readily traced up into the crater. At four filled craters, numerous sand-filled vents can be traced downward from the base of the crater and through the underlying C horizon into the sediments beneath. The vents are traceable as zones of massive sand cutting steeply through sand containing nearly horizontal, thin primary beds of black heavy minerals.

Other origins considered for the craters but rejected include liquefaction caused by landslides or storm wave loads and primary or dewatering sedimentary structures, channels, springs, decayed stump and root holes, and blown-down root-wadded trees. The filled craters have physical properties consistent only with the historic descriptions of the formation and filling of earthquake-induced sand-blow craters (5, 8, 9) and their inferred mechanical processes.

Three independent types of evidence indicate that the filled craters predate 1886:

1) The filled craters typically have dense humate-rich solums 25 to 75 cm thick. In contrast, the ejection blanket of the 1886 sand blow excavated by Cox and Talwani (8) has only a weak A horizon in its upper 15 cm. This large difference in solum development is qualitative evidence for a large age difference between the features at these sites.

2) Carbon-14 dating yielded apparent ages of 1380 ± 120 years for a Bh horizon developed above one crater and 4680 ± 150 years on large Bh clasts within the lower part of the same crater. The age of 1380 years presumably represents carbon fixation in the time period from after formation of the crater until the present and is a minimum age for crater development. The age of 4680 years represents carbon fixation in soil before crater development and is a maximum age.

3) Thin, sand-filled fissures cut across filled craters and undisturbed parts of the solum at three sites in the Hollywood ditch (6). The fissures, commonly 1 to 2 cm wide but locally expanded to 10 cm, contain light yellow, micaceous quartz sand. Their exposed lengths range from a few centimeters to more than 5 m. One fissure widens downward and extends to the ditch bottom; the other two are roughly parabolic in cross-sectional view on the ditch wall. The fissures extend into the ditch bank at least 0.3 m (the maximum excavated depth) and thus have dike- or sill-like geometries. We interpret these fissures as earthquake-induced, liquefaction-flowage features similar to small sand fissures (clastic dikes) produced elsewhere by historic earthquakes (9). The fissure sands in the Hollywood ditch do not show any evidence of humate accumulation or other alteration. Therefore, the sands were injected during a recent earthquake, probably the 1886 earthquake. Because all three thin fissures physically cut across weathered filled craters, because the fissures represent a recent earthquake, and because no historic earthquake at Charleston other than the 1886 event produced liquefaction-related features, the large filled craters must represent prehistoric earthquakes.

At one site in the Hollywood ditch, a large Y-shaped crater cuts across all sediment units within a larger U-shaped crater (Fig. 2d); the Y-shaped crater clearly is younger. The Bh horizon is slightly thinner above the Y-shaped crater than above the U-shaped crater, but the difference is too small to permit reliable age comparison. The Y-shaped crater might represent a large aftershock of the earthquake that produced the U-shaped crater; alternatively, the Y-shaped crater could have formed a few hundreds to thousands of years after the formation of the older crater.

In summary, the large, sand-filled craters predate the 1886 earthquake and the 300-year recorded history of the Charleston area. The numerous craters in the Hollywood ditch may represent many earthquakes, but only two prehistoric events presently can be documented (Fig. 2d).

As sediments age, cohesive bonds develop at grain-to-grain contacts and cause increased resistance to liquefaction. Sediment types at the Hollywood ditch, when older than about 15,000 years and less than a million years, typically have low to very low susceptibility (10). Because the Hollywood craters formed through a soil profile that yielded ¹⁴C residence times of about 23,000

years at its base, moderate to strong earthquake shaking was almost certainly required for liquefaction. Another line of evidence is provided by crater size. Craters in the Hollywood ditch are comparable in size to 1886 craters that are developed in similar materials; this suggests comparable shaking intensities.

Ten years ago the 1886 Charleston earthquake generally was viewed as the product of a local, unique seismotectonic setting. After a decade of extensive work on Charleston and southeastern seismicity, many workers have changed their opinions and they now no longer consider Charleston tectonically or seismotectonically unique in the Southeast (11). In a narrow context, the present study supports the concept of a unique seismotectonic setting at Charleston. That is, the evidence for several moderate to large Quaternary earthquakes near Charleston contrasts with the absence of evidence for similar Quaternary earthquakes elsewhere in the Southeast. However, this absence of evidence results primarily from a lack of adequate study, and it is possible that extensive regional searches for earthquake-induced, liquefaction-related features in Quaternary sediments could significantly extend the known distribution of seismicity in the Southeast.

STEPHEN F. OBERMEIER
GREGORY S. GOHN
ROBERT E. WEEMS
ROBERT L. GELINAS
MEYER RUBIN

U.S. Geological Survey,
926 National Center,
Reston, Virginia 22092

References and Notes

1. C. E. Dutton, "U.S. Geological Survey Ninth Annual Report of the Director, 1887-1888" (1889).
2. O. W. Nuttli, *U.S. Geol. Surv. Open-File Rep. 83-843* (1983), pp. 44-50; G. A. Bollinger, *U.S. Geol. Surv. Prof. Pap. 1028* (1977), pp. 17-32. Intensity X effects occurred in the epicentral area northwest of Charleston, and intensity IX effects occurred in the city. Structural damage (modified Mercalli intensity VIII effects) resulted as far as 250 km from Charleston; 60 to 110 deaths have been attributed to this earthquake.
3. Tectonic and seismologic studies of the greater Charleston area are contained in the following: D. W. Rankin, Ed., *U.S. Geol. Surv. Prof. Pap. 1028* (1977); G. S. Gohn, Ed., *U.S. Geol. Surv. Prof. Pap. 1313* (1983); W. W. Hays and P. L. Gori, Eds., *U.S. Geol. Surv. Open-File Rep. 83-843* (1983).
4. C. W. Wentworth and M. Mergner-Keefer, in *Earthquakes and Earthquake Engineering: The Eastern United States*, J. M. Beavers, Ed. (Ann Arbor Science, Ann Arbor, Mich., 1981), p. 109.
5. Liquefaction is "the transformation of a granular material from a solid state into a liquefied state as a consequence of increased pore-water pressures" [T. L. Youd, *U.S. Geol. Surv. Circ. 688* (1973), p. 10]. In the liquefied state, the material behaves basically as a fluid mass. The increased pore-water pressure is induced by earthquake shaking. During shaking, generally within 15 m of the ground surface, the pore pressure increases in relatively loose granular materials as they are deformed [H. B. Seed, *ASCE J. Geotech. Eng. Div.* **105** (No. GT2), 201 (1979)]. A high pore pressure can remain after shaking and migrate upward, causing liquefac-

- tion and venting to the surface of the fluidized mass, thus inducing sand blows.
6. G. S. Gohn, R. E. Weems, S. F. Obermeier, R. L. Gelinis, *U.S. Geol. Surv. Open-File Rep.* 84-670 (1984).
 7. L. Seeber and J. G. Armbruster, *J. Geophys. Res.* 86, 7874 (1981); *U.S. Geol. Surv. Open-File Rep.* 83-843 (1983), p. 142.
 8. J. Cox and P. Talwani, *Geol. Soc. Am. Abstr. Programs* 15 (No. 2), 65 (1983); *Seismol. Soc. Am. East. Sect. Earthquake Notes* 54 (No. 3), 16 (1983); *Geol. Soc. Am. Abstr. Programs* 16 (No. 3), 130 (1984); J. H. M. Cox, thesis, University of South Carolina, Columbia (1984).
 9. S. G. Muir and S. F. Scott, *U.S. Geol. Surv. Prof. Pap.* 1254 (1982), pp. 247-250; H. W.

- Coulter and R. R. Migliaccio, *U.S. Geol. Surv. Prof. Pap.* 542-C (1966); G. Plafker and R. Kachadoorian, *U.S. Geol. Surv. Prof. Pap.* 543-D (1966).
10. T. L. Youd and S. N. Hoose, in *Proceedings, 6th World Conference on Earthquake Engineering* (Sarita Prakashan, Meerut, India, 1977), pp. 2189-2194.
11. C. M. Wentworth, *U.S. Geol. Surv. Open-File Rep.* 83-843 (1983), pp. 266-275.
12. Research by the U.S. Geological Survey in the Charleston, S.C., area is supported by the U.S. Nuclear Regulatory Commission under agreement AT(49-25)-1000.

7 August 1984; accepted 1 November 1984

Highly Supercooled Cirrus Cloud Water: Confirmation and Climatic Implications

Abstract. *Liquid cloud droplets supercooled to temperatures approaching -40°C have been detected at the base of a cirrostratus cloud through a combination of ground-based, polarization laser radar (lidar) and in situ aircraft measurements. Solar and thermal infrared radiative budget calculations based on these observations indicate that significant changes in the atmospheric heating distribution and the surface radiative budget may be attributed to liquid layers in cirrus clouds.*

The meteorological classification of atmospheric clouds is based on the mechanism of cloud formation, as reflected in their appearance and spatial structure, and these cloud categories are then subdivided according to cloud altitude. Since temperatures decrease steadily with height in the troposphere, this grouping into low, middle, and high clouds is pertinent to the thermodynamic phase of the clouds under standard atmospheric conditions. Although water droplets can exist at temperatures well below 0°C , the probability that a supercooled cloud will glaciate increases rapidly with decreasing temperature. If cloud droplets are composed of pure water, a small drop will likely remain in a supercooled state until its temperature approaches the spontaneous freezing point of water, about -40°C , before homogeneous nucleation occurs (1). However, special particles, or ice nuclei, that are capable of initiating heterogeneous nucleation at much warmer temperatures are usually present in the atmosphere. Measurements of natural ice nuclei in the lower atmosphere show a strong temperature dependence. Particles that are active at temperatures warmer than about -10°C are relatively scarce, but with decreasing temperatures the concentrations of ice nuclei increase exponentially (2).

Since the family of cirrus clouds occurs in the upper troposphere, even extending to the tropopause where temperatures are extremely cold (-50° to -60°C), cirrus clouds are commonly thought to be composed of ice crystals. Indeed, it seems implicit in the definition of cirrus clouds that liquid water, in any

measurable amounts, should be absent. Recent evidence provided by remote sensing observations, however, would indicate that cloud liquid water can exist in a highly supercooled state within the temperature range typical of at least the lower cloud regions of cirrus clouds (3-5). To account for these observations, it has been suggested that impurities from hygroscopic cloud condensation nuclei, such as ammonium sulfate, depress the homogeneous freezing temperature (3) and that ice nuclei derived from the earth's surface are uncommon at such great altitudes (4).

A field research program, designed in part to test the hypothesis that highly supercooled water can be present in cirrus clouds and can play a significant role

in their formation and radiative properties, was recently carried out in the vicinity of the Colorado Front Range near Boulder, Colorado. Measurements were made with a ground-based ruby lidar system (6), and a specially instrumented jet aircraft designed to provide in situ measurements of cirrus cloud content was used. The Sabreliner research aircraft of the National Center for Atmospheric Research (NCAR) was equipped with a number of probes to measure the sizes and concentrations of both ice crystals and cloud droplets and to routinely record other pertinent information such as the upward and downward fluxes of solar and terrestrial radiation (7). With the polarization technique used by the lidar, cloud droplets can be discriminated from ice crystals through the use of the linear depolarization ratio δ , defined as the ratio of the backscattered laser power in the plane of polarization orthogonal to the linearly polarized source divided by the backscattered laser power in the plane of polarization parallel to the source. This capability is a consequence of the principle that spherical particles (for example, cloud droplets) do not depolarize the incident electromagnetic waves during single scattering, whereas nonspherical scatterers such as ice crystals introduce a depolarized component into the backscattering.

Verification of the presence of highly supercooled cirrus cloud water was obtained from an approximately 2-km-thick, layered cirrostratus cloud on 17 October 1983. The lidar returns indicated a liquid cloud signature at the 8.5-km base (above mean sea level) of the cirrus layer at 1735 G.M.T. (Fig. 1). The aircraft was subsequently directed to sam-

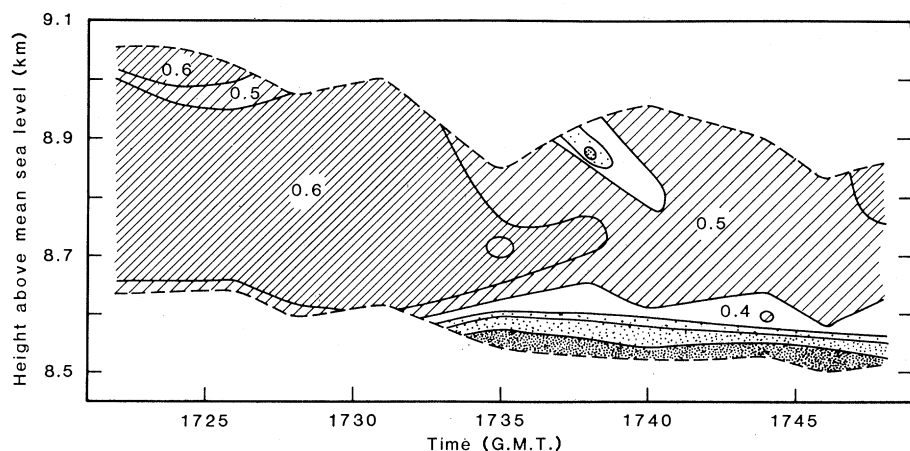


Fig. 1. Height versus time display of linear depolarization ratios generated from vertically pointing lidar measurements during the initial appearance of highly supercooled liquid water at the bottom of a 2-km-thick cirrostratus cloud on 17 October 1983. A gradual water-to-ice cloud transformation is shown by the decreasing stippling just above the cloud base. The cloud boundaries (dashed lines) derived from the δ value analysis often do not correspond to the actual cloud boundaries, particularly in the presence of significant optical attenuation.